Second Joint Meeting of the United States Sections of the Combustion Institute

Particle Image Velocimetry in Flickering Methane/Air Diffusion Flames

George Papadopoulos

Dantec Measurement Technology, Inc.
Mahwah, NJ 07430

and

Rodney A. Bryant and William M. Pitts

Building and Fire Research Laboratory
National Institute of Standards and Technology
Gaithersburg, MD 20899

ABSTRACT

Phase-resolved measurements of the velocity field in acoustically forced, flickering laminar co-flowing methane/air diffusion flames have been made. Identical flames have been studied extensively in the past in order to characterize the effects of the vortical structures responsible for the flicker on the flame structure, but the initial velocity perturbation and the velocity fields have not been reported previously. Phase-locked measurements of the instantaneous two-dimensional velocity field at ten phases within a full excitation cycle were made using particle image velocimetry. The velocity measurements were complemented by phase-resolved shadowgraphs recorded in the vicinity of the flame base. Measurements are reported for the two forcing conditions that have most often been studied for this burner. When integrated with the results of previous studies, these measurements provide a clearer picture of the interactions between the buoyancy-induced vortical structures and the flame sheets, as well as, providing an understanding of the initial conditions required for realistic modeling of these flames.

1. INTRODUCTION

Vortex interactions with flames play a key role in many practical combustion applications and, as a result, have been the focus of considerable study.[1] Such interactions form the basis of understanding in naturally flickering buoyancy-dominated diffusion flames. These flames exhibit natural flicker as a result of a buoyancy-induced flow instability, which leads to the formation of strong vortical motions that subsequently interact with the combusting regions of the flame.[2-4] Under normal gravity conditions, the flames have a well defined oscillation frequency that is inversely proportional to the square root of the burner diameter, D, and to a good approximation can be written as $f \approx 1.5D^{1/2}$, with D given in meters. Despite the widespread natural occurrence of flame flickering, however, much of our current understanding of diffusion flame behavior is based on the experimental characterization of steady laminar flames. Detailed characterization of flickering flames is considerably more limited. This limitation is significant because ranges of flame properties, such as local strain and scalar dissipation rates and flame residence times, are significantly broader in laminar time-varying diffusion flames than in steady flames. A better

understanding of flickering flame behavior also promises to improve the current understanding of turbulent combustion systems since a much wider range of local conditions is available to characterize the flame-flow interactions that are characteristic of turbulent flames.

Naturally occurring flickering flames are difficult to investigate experimentally because, even though the flickering frequency is well defined, there exist cycle-to-cycle variations. These variations lead to spatial and temporal averaging with a resulting loss in resolution, since it is usually not possible to record local experimental measurements throughout the flame during a single cycle. Conditional sampling (e.g., see Ref. 5) provides some improvement, but significant averaging still occurs. It has been found that it is possible to generate very repeatable time-varying diffusion flames by acoustically forcing the fuel flow at frequencies close to their natural oscillation frequency.[6] Such flames can be characterized by repeated phase-averaged measurements. While not necessarily identical to the corresponding naturally flickering flame (acoustically forced flame structures are found to change with the degree of forcing), the flames are sufficiently similar to suggest that the governing physical mechanisms are the same. The ability to control the degree of forcing also offers an opportunity to control local flame conditions.

A seminal paper by Lewis et al. demonstrated the effectiveness of the approach.[7] The authors applied a variety of experimental techniques including flame imaging, laser-induced fluorescence imaging of the hydroxyl (OH) free radical and particle tracking velocimetry to demonstrate that flame flickering is associated with the formation of strong vortical structures having centers located outside of the flame sheet. They were also able to demonstrate that a flame extinction observed over small regions of their flame occurred at positions where the strain rate was sufficiently high to extinguish a steady laminar diffusion flame.

Over the past several years, numerous investigations concerning acoustically forced flickering flames have been reported on a modified burner originally developed at the National Institute of Standards and Technology (NIST) for steady laminar flame studies.[8] Phase-resolved measurements that have been reported include laser-induced fluorescence imaging of OH[9,10], CO[11], and polycyclic aromatics[12], flame luminosity[12], soot scattering[9,10], extinction[10], soot field characterization using laser-induced incandescence (LII)[13], temperature measurements along lines across the flame using time-resolved thin-filament pyrometry,[14,15] infrared tunable diode laser measurements of carbon monoxide[16], and characterization of local soot morphology within the flames[17]. Many of the NIST results are summarized in an extensive database available on the World Wide Web.[18] The experimental findings have been compared with a detailed two-dimensional modeling study designed to predict the flame structure and soot fields for the time-varying flame.[19]

Even though the experimental characterization of time-varying flames on the NIST burner is extensive, a major limitation for the data set up to now is that there have been no experimental measurements of the corresponding velocity fields or even of the initial flow conditions. Early attempts to quantify the initial flow conditions using bubble-flow meters and hot-wire anemometry were unsuccessful.[9] Two flow conditions, characterized by the amplitudes of the sinusoidal voltage applied to drive the loud speaker of the original NIST burner, 0.75 V and 1.5 V, have received the most attention in these previous studies. The general descriptors “moderate” and “strong”, respectively, were used to distinguish the two flame cases.

The present paper addresses the need for velocity field characterization of these time-varying flames by reporting phase-resolved particle image velocimetry (PIV) measurements for the two cases. In addition to PIV measurements, phase-resolved shadowgraphy was used to qualitatively investigate the refractive index field at the base of the flame, which was expected to correlate with the local temperature field, thus making apparent regions of cold fuel injection and ambient air entrainment

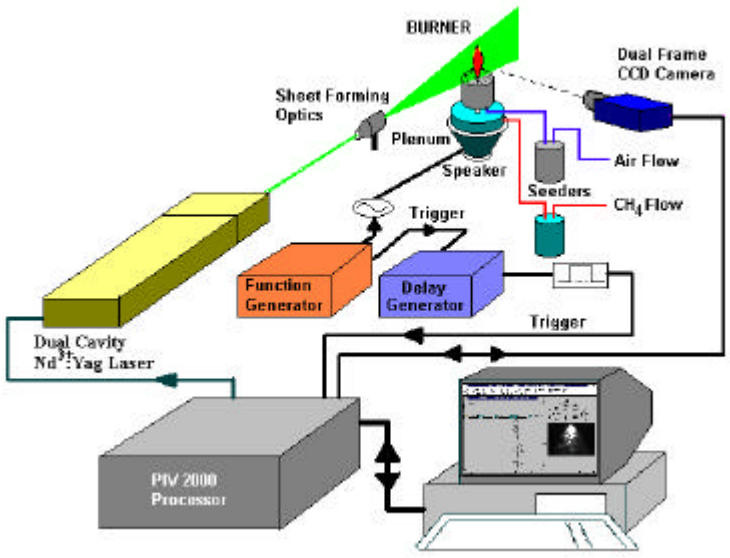

Figure 1. Experimental setup of burner and PIV instrumentation for carrying out velocity measurements in the time-varying flames.

2. EXPERIMENTAL SETUP

A schematic of the experimental arrangement is shown in Figure 1. A second burner, identical in material and design to the one used by Smyth and co-workers at NIST[9-15], was built for the purpose of carrying out the PIV measurements. The shadowgraph measurements were performed on the original burner, subsequent to a preliminary investigation designed to accurately match the two flame cases on each burner.

A. Burner Description

An unconfined, axisymmetric, laminar diffusion flame was established at atmospheric pressure on a co-annular burner consisting of an 11.1-mm-diameter fuel tube surrounded by a 101-mm-diameter air annulus. The 100-mm-tall air chamber was filled with glass beads, followed by several fine mesh screens and a 25.4-mm-thick ceramic honeycomb section with 1.5-mm-square cells. This arrangement was designed to provide an initially uniform flow velocity across the top of the annulus, as previously noted in earlier investigations using the same burner design. No beads or screens were used for flow conditioning in the 161-mm-long fuel tube. The tube was attached to a plenum below the air chamber, extending 6 mm into this plenum, and its exit was elevated 4 mm above the honeycomb. The plenum was 153 mm in diameter and 32 mm deep and was sealed on the bottom side with a 1-mm-thick rubber diaphragm.

A 20.3 cm (8-inch) standard speaker was mounted on the underside of the plenum to the bracket supporting the diaphragm. The speaker was sinusoidally excited using the voltage signal from a digital function generator. The excitation frequency was 10 Hz, and the output was set to the values (peak-to-peak measured at the speaker) appropriate for generating flames matching the previously investigated moderately and strongly forced flickering flames.

The fuel was “UCP”-grade methane, introduced into the plenum at a constant rate of 0.452 L/min. The resulting bulk velocity (assuming room temperature flow) at the exit of the fuel tube was 77.7 mm/s. House-supply air flowed through the annulus at a rate of 38.0 L/min, yielding an average velocity of 79.0

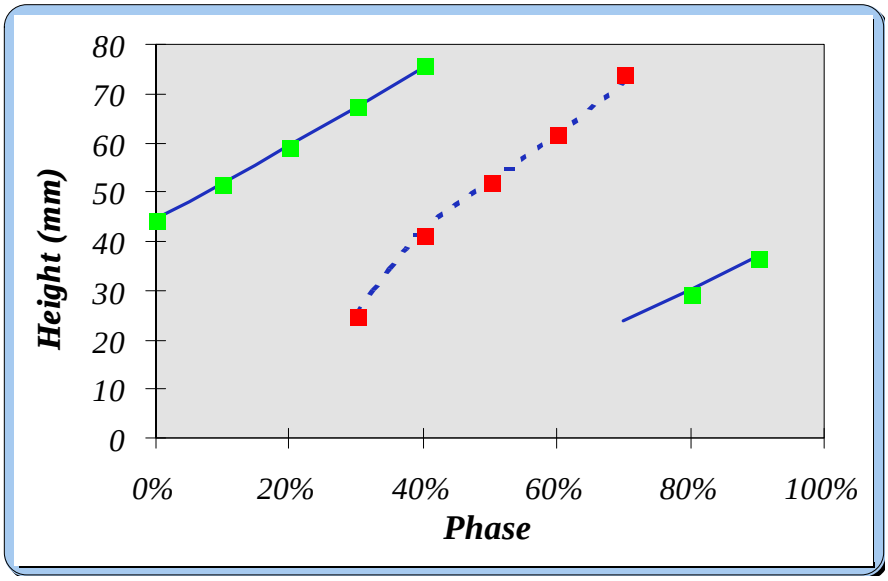

Figure 2. Visible flame heights for the strongly perturbed case determined from recorded images at each of the ten phases (symbols) are compared to the visible flame heights reported by Smyth et al.[9] (lines, dashed line corresponds to clipped flame base-height measurement).

mm/s across the top. Both fuel and co-flow air were regulated using mass-flow controllers separately calibrated for each fluid using a bubble flow meter. The calibration uncertainty of both controllers was less than 1%[†]. Under these steady-flow conditions the laminar diffusion flame had a visible height of 79 mm, in agreement with earlier measurements on the original burner.[9] Even though the original and new burners were nominally identical, it was found that the flames generated by applying 0.75 V and 1.5 V sine waves to the speaker for the new burner differed significantly from the moderately and strongly forced flames previously investigated. A similar observation was reported by Skaggs and Miller and attributed to subtle differences in the way the rubber diaphragm was installed.[16] By systematically varying the applied voltage of the sine wave for the new burner and comparing flame images for different phase angles, conditions were identified that provided nearly identical flames for the moderate and strong forcing conditions. As a demonstration of the success of this approach, Figure 2 shows a comparison of the visible flame heights for the split flame as well as the base of the upper flame (see Fig. 3) for the strong forcing case recorded using the two burners. The comparison is quite good. Results shown in Smyth et al. indicate that the flame shapes depend strongly on the voltage of the applied sine wave, providing additional evidence that the initial conditions for the cases on both burners are closely matched.[9] Examples of flame luminosity results collected during the present investigation for the strongly perturbed flame are shown in Figure 3. The images were obtained using the digital camera setup that was part of the PIV instrumentation described in detail in the following section. A Schott BG-12 filter was placed in front of the lens to limit wavelength detection to the visible spectrum below approximately 530 nm. Only the strong radiation from soot particles is detected in this wavelength region, thus allowing comparison with similar images reported by Smyth et al.[12]

B. PIV System and Data Analysis

A commercial PIV system was used consisting of a laser illumination source, digital imaging device, and dedicated hardware and software for data analysis. The illumination source was a frequency-doubled, double-cavity Nd:YAG laser operating at a wavelength of 532 nm (200 mJ per pulse) and a pulse rate of 15 Hz. The overlapped core beams were expanded into a 20-degree diverging light sheet using focusable

[†] Reported uncertainties are at 95% confidence, unless otherwise noted.

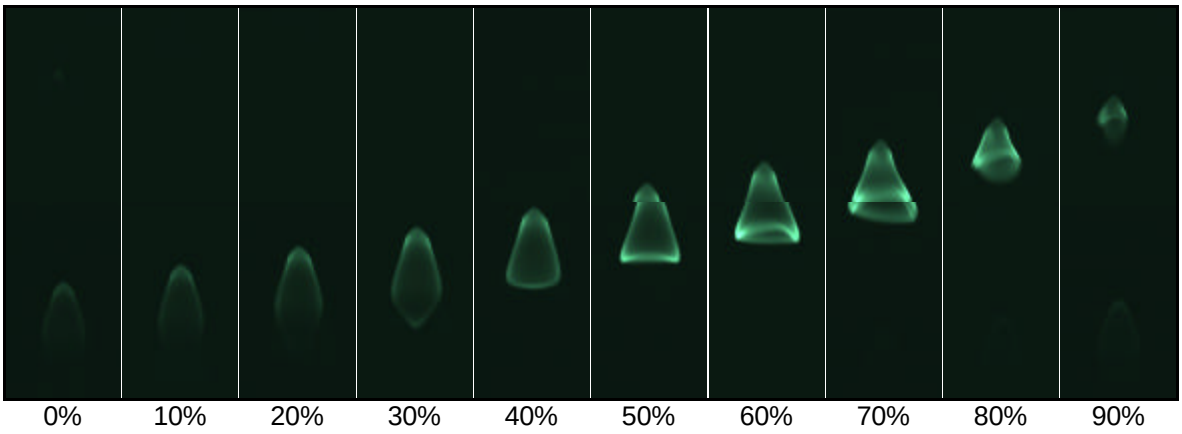

Figure 3. Visible luminosity images for the strongly flickering flame case, obtained with a Schott BG-12 filter and 1-ms shutter window (images are gray scale reversed; each image size is 47.6-mm wide by 160.7-mm high)

sheet-forming optics. At the measurement station, the sheet was approximately 1 mm thick and was aligned vertically along the diameter of the fuel tube (as shown in Figure 1). Recording of particle image pairs was accomplished via an 8-bit double-frame CCD camera having a resolution of 1008 x 1018 pixels. This type of camera eliminated image-order ambiguity and allowed for the use of cross-correlation methods when determining velocity vectors. A bandpass filter centered at 532 nm (±15 nm) was placed in front of the camera lens to reduce flame luminosity effects on the acquired images. Processing of the images to derive vector maps was done via dedicated hardware for on-line correlation analysis by means of FFT-based algorithms implemented using programmable electronics. The correlator was housed inside a processor unit that contained a memory buffer and camera personality module, as well as, a synchronization module for phase-locking the laser and camera activation sequences to an external trigger source. Once evaluated, a raw vector map data was passed to a personal computer for visualization and storage. Setting of data acquisition parameters and management of data was accomplished using dedicated software to interact with the programmable processor.

Seeding of the methane fuel and air co-flow was accomplished with 1.5-μm Al_2O_3 particles introduced into the flow lines using separate cyclone seeders located downstream of the mass-flow controllers. The seeders were equipped with bypasses to allow control of the seeding density. Seeding was initiated just prior to each data acquisition sequence to reduce particle accumulation in the burner annulus. During the course of the investigation the burner was regularly flushed with clean air to discharge accumulated particles and minimize blockage effects on co-flow velocity uniformity.

A 40-mm-square viewing area was sampled along the centerplane of the flame in individual experiments. Separate velocity maps were recorded at two heights by traversing the burner relative to the imaging system in order to cover a total distance of 80 mm in the axial direction. A trigger-out signal from the function generator was input into a digital delay generator, which in turn was used to trigger the PIV processor at fixed phase delays within the excitation cycle. Upon receiving the external trigger from the delay generator, the PIV processor synchronized laser pulse activation and image capture within a 100-ns time window. Four externally triggered ensembles of 18 recordings were acquired for each of the ten phases. The time separation between pulses was typically about 600 μs, yielding particle displacements of 15% to 20% of the square interrogation area length. A 64 x 64 pixel interrogation area at 50% overlap was selected, giving good dynamic range and signal-to-noise performance, with reasonable spatial resolution (approximately 2 mm). A peak-validation and moving average technique[20] were used to invalidate erroneous vectors prior to phase-averaging all 72 instantaneous realizations.

To investigate the initial conditions at the fuel tube exit, the camera was zoomed to a 20-mm-square area surrounding the exit. Seeding conditions were more favorable close to the exit, allowing for a 32 x 32 pixel interrogation area to be used for correlating particle displacement information between successive images. This resulted in a spatial resolution of approximately 0.6 mm. Relative particle displacements were maintained at 15% to 20% of the interrogation area size, yielding an estimated dynamic range of about 400 if an ideal sub-pixel resolution of 1/64 of a pixel is assumed. Realistically, seeding particle density and homogeneity and image contrast reduce the accuracy of displacement vector estimation, and as a conservative estimate a velocity resolution of at most 1/200-th of the maximum measured is assumed for all of the measurements reported herein. This corresponds to a minimum resolved velocity of approximately 1 cm/s and 2 mm/s for the field and inlet measurements, respectively. For each flame condition and at each phase an ensemble of 36 instantaneous, phase-resolved measurements at the exit of the burner were averaged to construct mean profiles of the vertical and lateral velocities, *W* and *U*, respectively.

C. Shadowgraphy

Prior to initiating the PIV measurements, the PIV apparatus was re-arranged to qualitatively investigate the refractive index field of each flame case using simple shadowgraphy. These measurements were performed on the original burner used by Smyth and co-workers.[9-15] Instead of using the sheet forming optics to illuminate a diametric plane, the laser beam was first expanded and then focused onto a 2-mm glass sphere which served as the point source for the shadowgraph. Scattered light from the sphere was then selectively collimated to a diameter of 50 mm and projected through the flame onto a screen located 190 cm from the center of the burner. Imaging of the shadowgraph was then performed using the CCD camera.

3. RESULTS

Vector plots of the centerplane velocity field obtained using the PIV technique are shown in Figure 4 and Figure 5 for the moderately and strongly flickering flame cases, respectively. Each vector map is the statistical average of 72 phase-resolved realizations, arranged to correspond with the phases for the OH radical and soot scattering images reported previously by Shaddix et al.[10] and shown in Figure 6 for comparison. The color-coding on the vectors denotes the velocity magnitude of each, while their length is shown as constant in order to better view vector orientation.

The flow is buoyancy driven as clearly indicated by the velocity magnitude. Maximum velocities during certain phases of the cycle exceed 1.8 m/s, more than 23 times the nominal bulk flow velocity of the fuel at the burner exit. Such high velocities are noticeable in areas above the instantaneous flame tip where a strong inward flow of surrounding gases is taking place. Comparable velocities are measured for both cases.

In the modeling efforts of Kaplan et al.[19], numerical tracking of fluid parcels in the flow field passing through the maximum sooting region showed that flickering flames exhibit much longer residence times during which the local temperature and stoichiometries are favorable for soot production. Good quantitative agreement between computations and experiments was achieved at mid-flame heights, but discrepancies existed near the burner lip. These discrepancies were attributed to several factors, but a potentially important factor not discussed was the selection of initial conditions at the exit of the fuel tube. In the absence of detailed measurements in this region, parabolic pipe flow was assumed and a 10-Hz sinusoidal function of varying amplitude (a 75% velocity variation was found to provide the best agreement with experiments) was applied to the fuel inflow velocity.

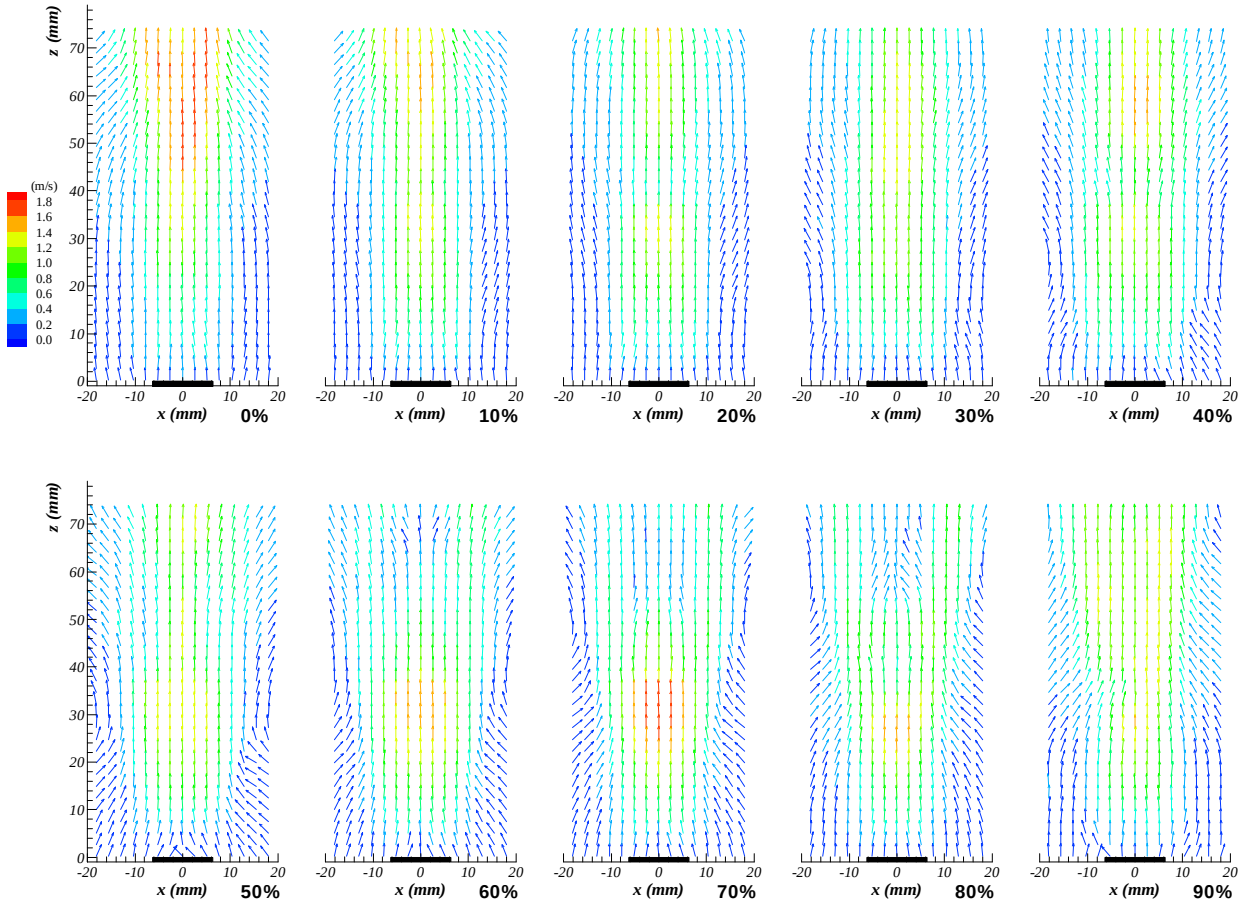

Figure 4. Vector plots of phase-averaged velocity in the plane of measurement for the moderately flickering flame case: results from 10 phases in an excitation cycle, starting with 0% at upper left, and increasing to the right (every other vector is shown for clarity).

In order to better characterize the initial flow conditions, detailed measurements of the velocity profile near the fuel tube exit (0.8 mm above) were performed during the present PIV investigation. The results of these measurements are shown in Figure 7 and Figure 8 for the moderate and strong cases, respectively. Several interesting features can be identified by considering the vertical velocity components, *W*, for the two cases. As expected under no-slip flow conditions, axial velocities approach zero for the boundary-layer locations near the burner wall. Interestingly, axial flow velocities immediately outside of the burner walls are increasing as the wall is approached. These velocities depend only weakly on phase angle. The flow acceleration is likely due to entrainment associated with the presence of an attached flame on the burner. The fuel tube extended 4 mm above the honeycomb, so it favored such an attachment. Signs of an attached flame present at the lip of the fuel tube are also visible in the shadowgraph images to be discussed a bit later.

For both cases the velocity profiles above the fuel tube vary dramatically with phase angle. During times when the velocities are decreasing the profiles have contours similar to those expected for parabolic flow. However, when the flow velocities begin to increase the profiles become strongly distorted with velocities near the center becoming lower than observed at more distant radial positions. For certain phases in both flames simultaneous in-flow and out-flow occur at different radial locations. Clearly, a parabolic flow profile is a poor approximation for the actual radial profiles present during these phases.

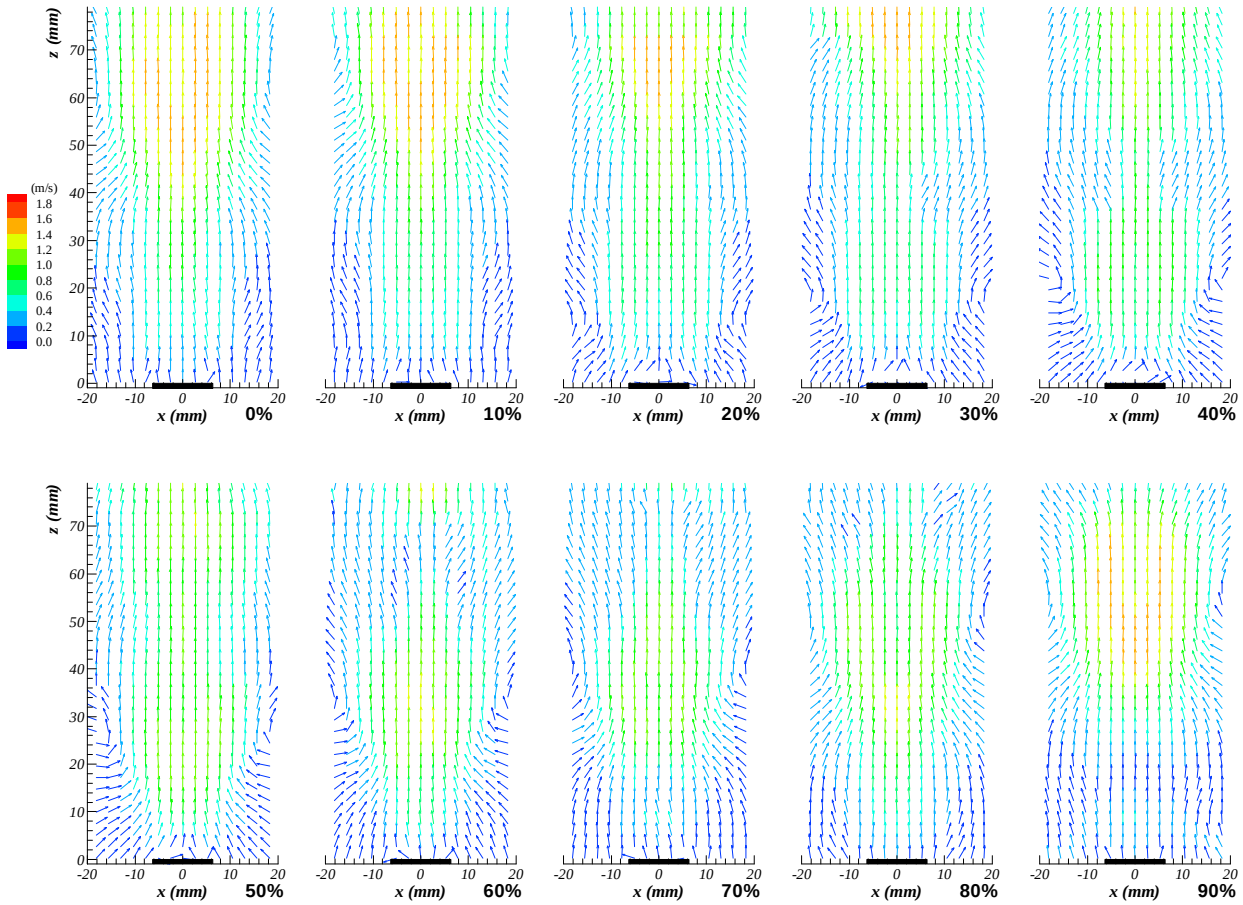

Figure 5. Vector plots of phase-averaged velocity in the plane of measurement for the strongly flickering flame case: results from 10 phases in an excitation cycle, starting with 0% at upper left, and increasing to the right (every other vector is shown for clarity).

Note that the phases corresponding to lowest and highest observed velocities differ significantly for the moderately (60% and 0%, respectively) and strongly (30% and 80%, respectively) forced flames. During certain phases, especially for the strongly forced case, negative *W* velocities are measured, indicating that fluid is actually being sucked back into the fuel tube. The highest negative velocities (approximately 2 times the nominal bulk velocity) for the strongly forced flame are recorded for the 30% phase, which corresponds to the time in the cycle when the flame tip is about to clip (see Figure 6). Much lower negative velocities are recorded for the moderately forcing case with the most negative velocity also corresponding to the phase when the flame tip is about to clip. Maximum observed velocities for the two cases are roughly three and four and a half times higher than the nominal bulk velocity for moderate and strong forcing, respectively.

The flow behaviors indicated by the near-field axial velocity component measurements are qualitatively confirmed by phase-resolved shadowgraphs generated at the base of the flame and shown in Figure 9 and Figure 10 for the moderate and strong cases, respectively. A shadowgraph is sensitive to the second derivative of the index-of-refraction, which near the flame base is primarily indicative of the temperature gradient field. Cooler regions are emphasized more strongly in the shadowgraphs. The injection of cool fuel at the base of the flame can be clearly seen in the shadowgraphs during phases when the flow velocities are increasing (phases 70% to 0% for the moderate case and 60% to 90% for the strong case). In addition, the shadowgraphs show clearly the clipping and lifting process the flames undergo during a

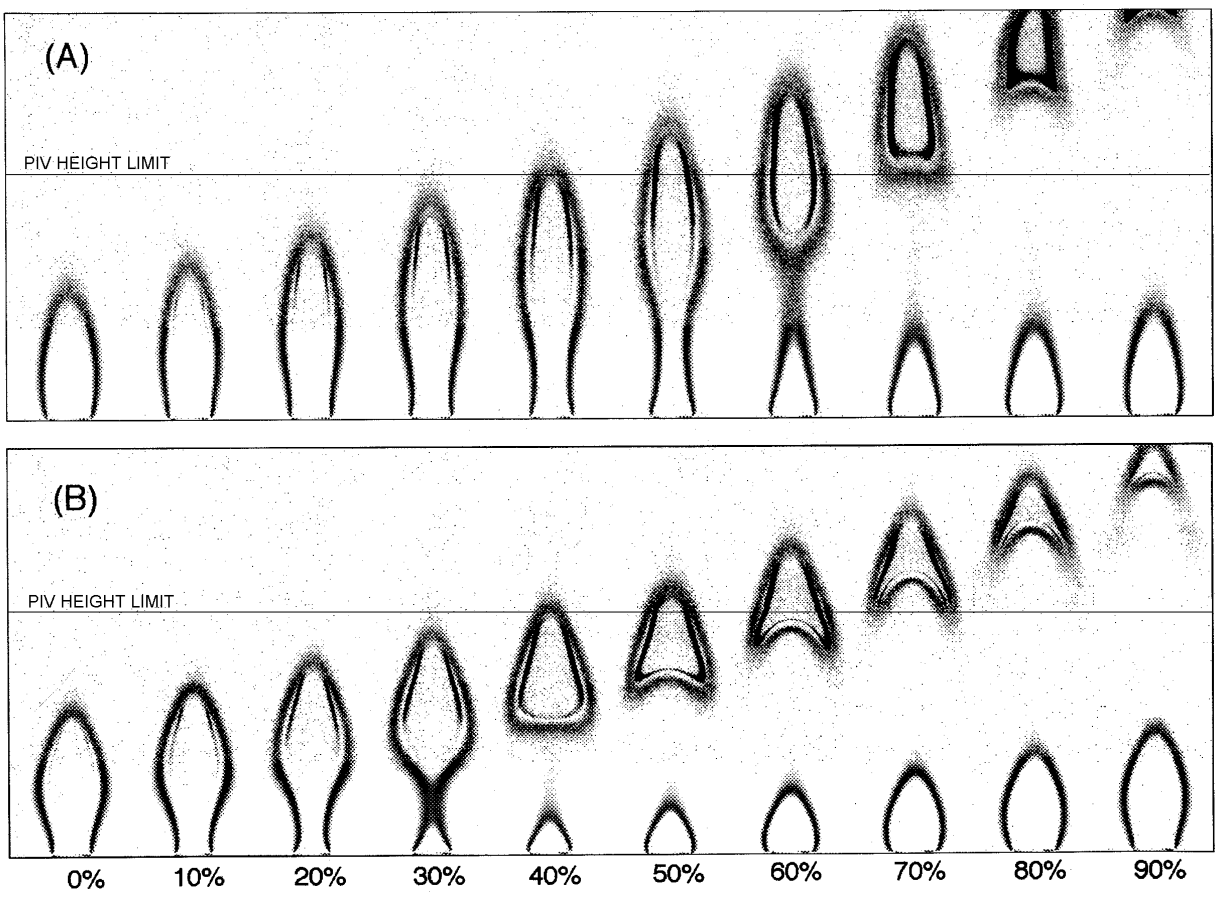

Figure 6. OH · laser-induced fluorescence and soot scattering images reported previously by Shaddix et al.[10]: (A) is moderately flickering flame case; (B) is strongly flickering flame case.

cycle of the excitation. Heated gases are pushed towards the center as cool ambient air is drawn in. In both flames, clip off occurs when the diameter of the heated gases above the burner is near a minimum. Strong mixing of cool and hot regions is clearly visible in the shadowgraphs, especially at the bases of the clipped flames. Furthermore, in support of an attached flame at the lip of the fuel tube, the shadowgraphs show a continuous region of ray coalescence extending below the tube exit in most of the phases, which is indicative of a heated region lying below the exit level.

The radial components of the velocity profiles have different dependencies on radial position than observed for the axial components. For positions outside of the fuel tube the radial velocities depend quite strongly on phase angle, and the relative magnitudes fluctuate substantially. The profile behaviors are quite complex and show that the net radial flow direction varies from inward to outward during a cycle. As expected, the absolute magnitudes are considerably larger for the strongly forced condition. For regions immediately above the fuel tube the radial velocities also vary with phase, but the flow is generally always toward the centerline with the velocity magnitude decreasing as the flow approaches the centerline.

Streamline traces for the two forcing conditions investigated are shown in Figure 11 and Figure 12. The traces make obvious the existence of strong vortical rings (as indicated by the radial symmetry) that initially form near the bases of the flames and are then convected downstream with time. The vortical rings rotate from the high velocity side of the flow towards the low and in the process draw cool co-flow air towards the flame centerline. In doing so, they force the flame sheets towards the centerline. Flame

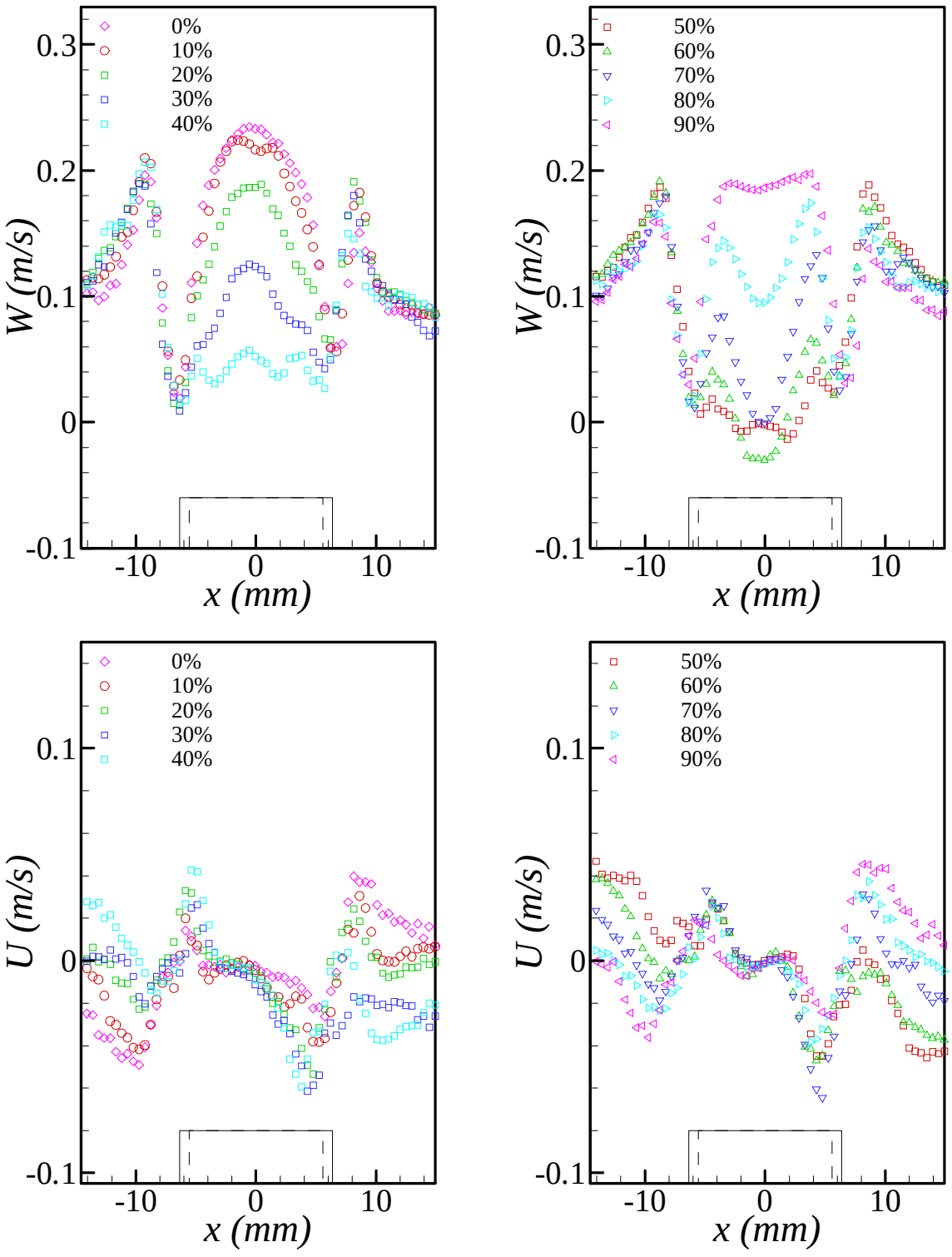

Figure 7. Velocity profiles near the exit of the burner (z = 0.8 mm) for the moderately flickering flame case.

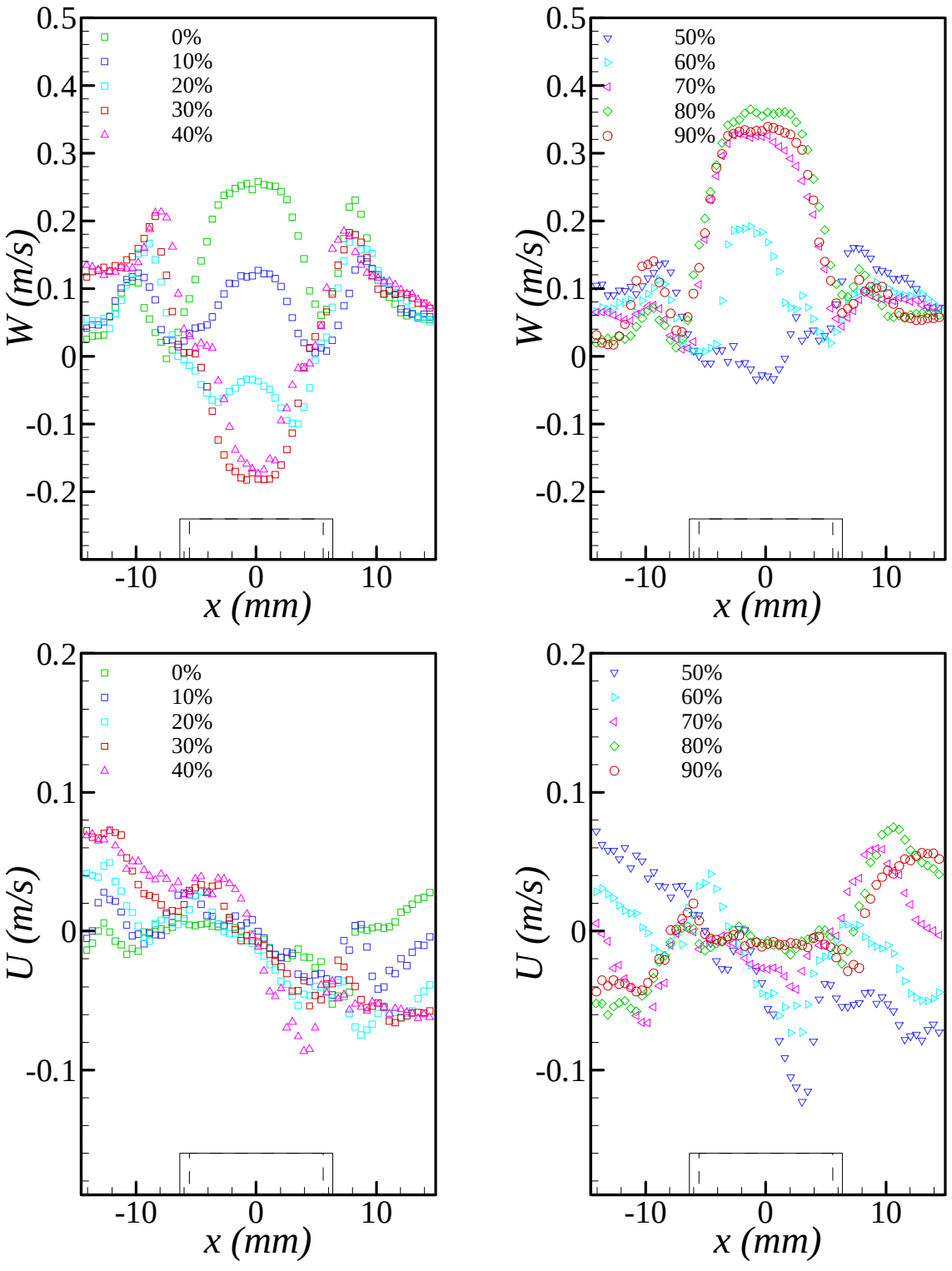

Figure 8. Velocity profiles near the exit of the burner (z = 0.8 mm) for the strongly flickering flame case.

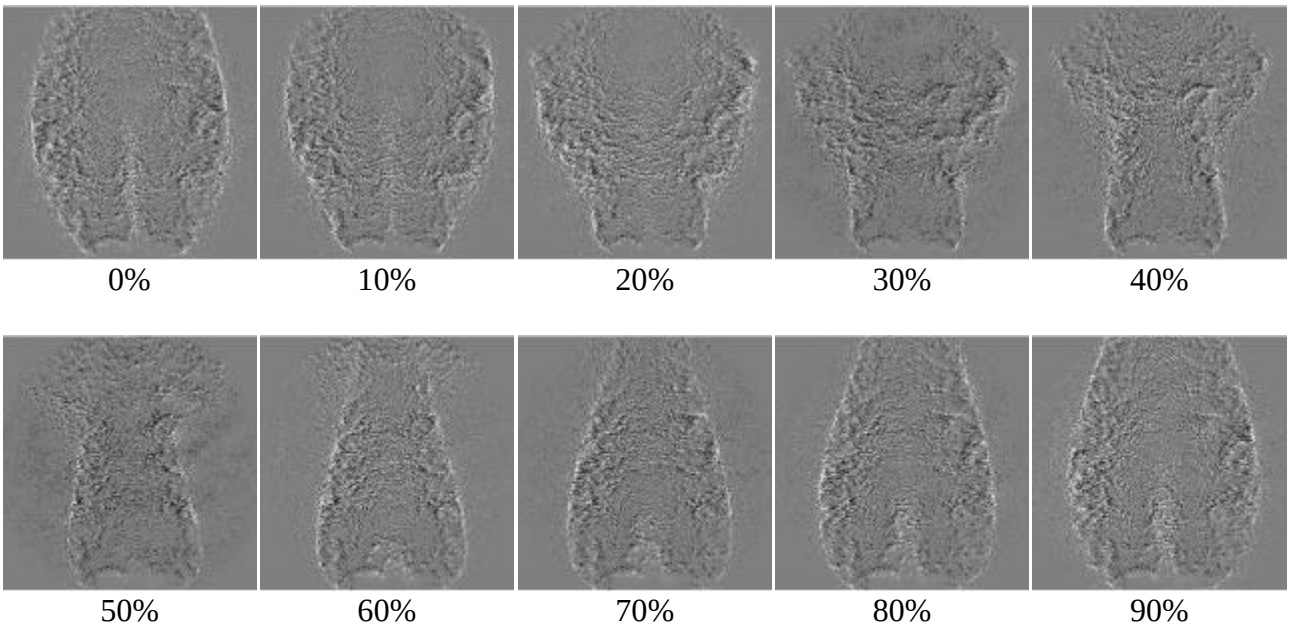

Figure 9 Shadowgraphs of the moderately flickering flame case.

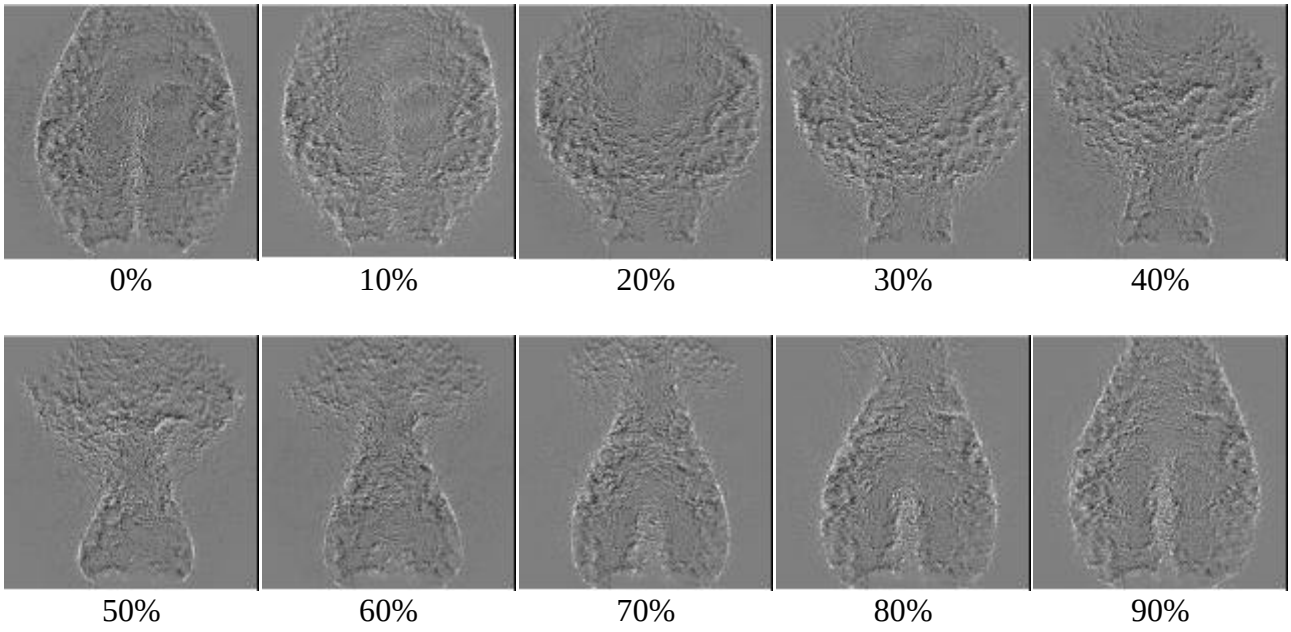

Figure 10. Shadowgraphs of the strongly flickering flame case.

clipping occurs when the entrained air reaches the jet centerline. As expected, maximum streamline deflections towards the centerline occur just before flame clipping, at phases of 60% and 40% for the moderate and strong forcing cases, respectively.

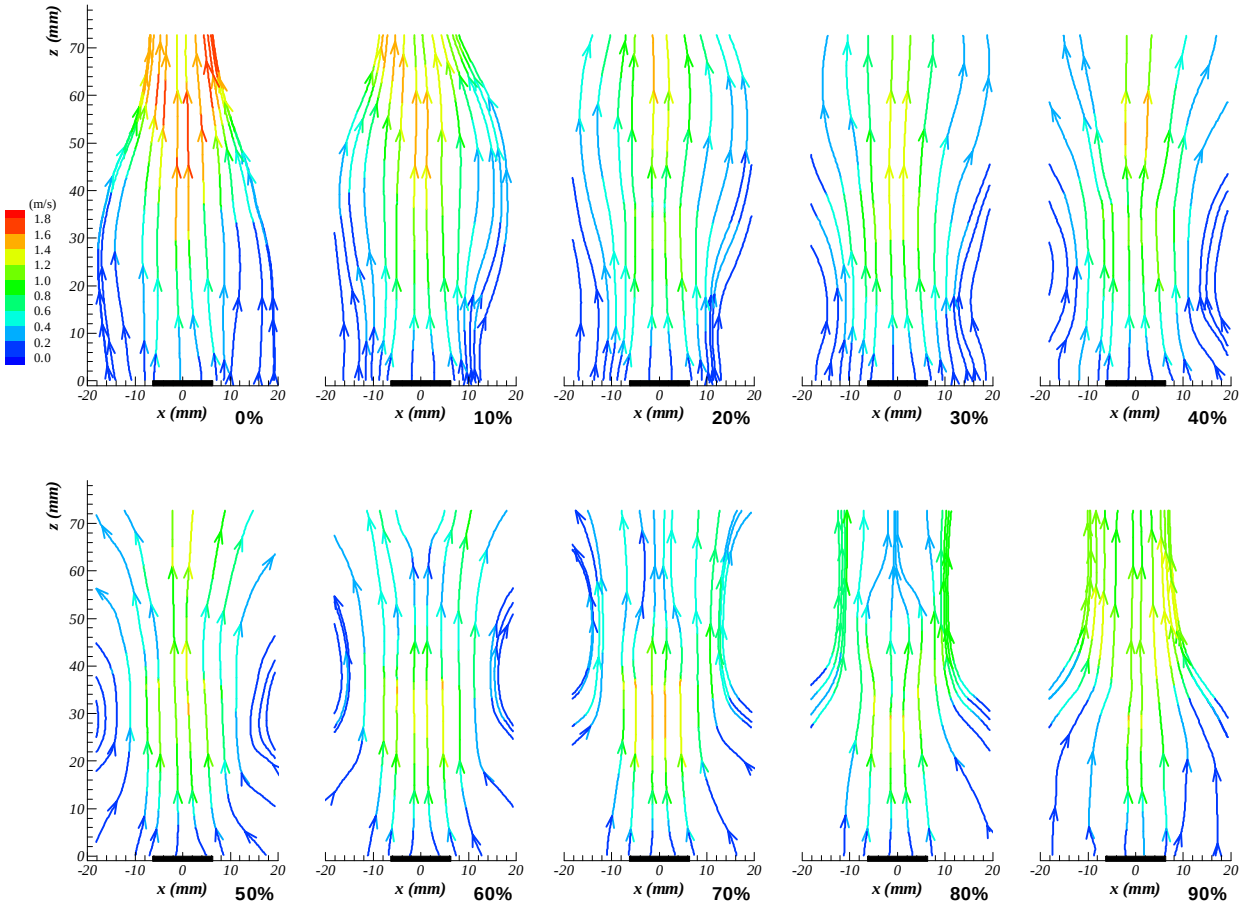

Figure 11 Streamline traces for the moderately flickering flame case, showing vortex-flow effect on the planar field: upper left data is for 0% phase; increasing phase is to the right.

The locations of the vortical centers responsible for the streamlines are outside of the regions imaged during the PIV measurements. Unfortunately, it was not possible to make measurements further from the centerline due to a fall off in seeding levels associated with entrainment of air from beyond the region of the coflow. Even so, it is clear that the vortical structures are centered in the surrounding coflow at positions well removed from the flow zone (compare the flame images in Fig. 6 with the streamline profiles in Figure 11 and Figure 12). It also appears likely that the distortions of the lower flame surfaces observed following flame splitting (see Fig. 6) result from interactions between the flame surface and these strong vortical structures.

Lewis et al. observed similar vortical structures during their investigation of acoustically forced laminar diffusion flames.[7] Full-phase-resolved measurements were not reported by these workers, so it was not possible to track the formation and growth of the structures. However, detailed comparisons with flame structure measurements did indicate that while the vortical structures were centered at locations well outside of the flame sheet, their influence did extend into the flame zone and were responsible for the distinct appearance at the base of the upper section of the split flame. Interestingly, the vortical structures in the Lewis et al. flame were sufficiently strong to induce strain rates that were high enough to extinguish the flame over small regions of the upper flame base. This was not observed for the current flames (see Figure 6).

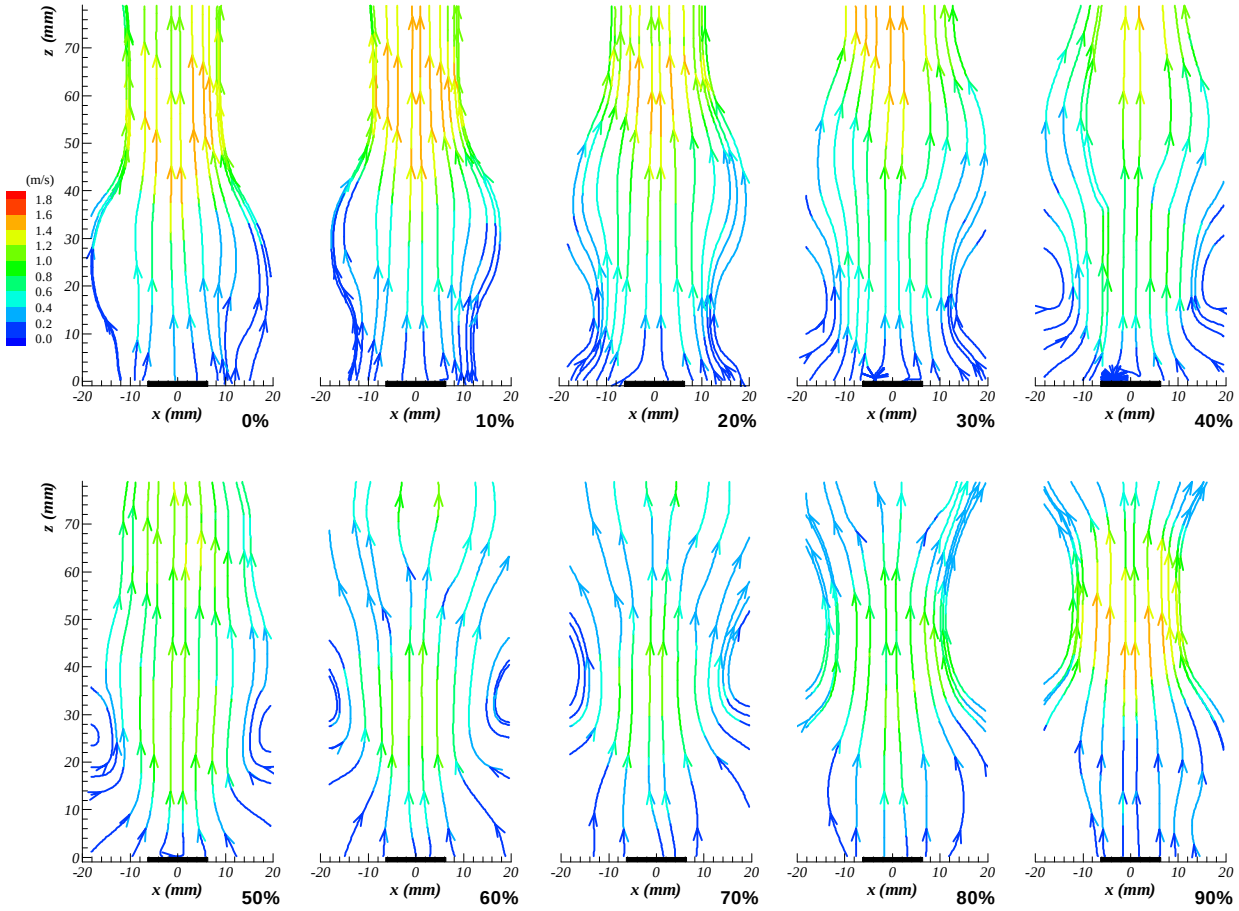

Figure 12. Streamline traces for the strongly flickering flame case, showing vortex-flow effect on the planar field: upper left data is for 0% phase; increasing phase is to the right.

4. CONCLUSIONS

Phase-locked measurements of the velocity field in the centerplane of an acoustically forced methane-air diffusion flame have been performed using PIV. These measurements complement an existing database of other phase-locked information recorded for the two flame cases considered herein. The results demonstrate the importance of vortical structures on the dynamics and topology of these flames.

The velocity profiles recorded nearest the burner provide the first quantification of the effects of acoustic forcing on the initial fuel flow velocity. The induced fluctuations are quite large relative to the time-averaged initial flow velocity, even becoming negative for significant fractions of the flame cycles. However, it is important to keep in mind that the fluctuations are relatively minor when compared with the ultimate velocities attained in these buoyancy-dominated flames. Perhaps of equal importance, forcing is shown to result in complex axial velocity profiles, which change dramatically with phase. Earlier modeling results for the moderate forcing case[19] were found to be highly sensitive to the initial velocity radial profile shape.[21] It is hoped that the improved characterization of the initial flow conditions provided by this work will lead to more realistic modeling of the flames and ultimately result in a better understanding of flow field/combustion coupling.

5. ACKNOWLEDGEMENTS

The measurements discussed herein were performed while the first author was a NRC Postdoctoral Fellow at the National Institute of Standards and Technology. The authors thank Dr. Kermit C. Smyth for numerous helpful comments and suggestions regarding this work.

6. REFERENCES

1. Renard, P.-H., Thévenin, D., Rolon, J. C., and Candel, S., "Dynamics of Flame/Vortex Interactions," *Progress in Energy and Combustion Science* **26** (2000) 225-282.
2. Hamins, A., Yang, J. C., and Kashiwagi, T., "An Experimental Investigation of the Pulsation Frequency of Flames," *Twenty-Fourth Symposium (International) on Combustion*, The Combustion Institute, Pittsburgh (1992) pp. 1695-1702.
3. Cetegen, B. M., and Ahmed, T. A., "Experiments on the Periodic Instability of Buoyant Plumes and Pool Fires", *Combustion and Flame* **93** (1993) 157-184.
4. Cetegen, B. M., and Dong, Y., "Experiments on the Instability Modes of Buoyant Diffusion Flames and Effects of Ambient Atmosphere on the Instabilities," *Experiments in Fluids* **28** (2000) 546-558.
5. Lingens, A., Reeker, M., and Schreiber, M., "Instability of Buoyant Diffusion Flames," *Experiments in Fluids* **20** (1996) 241-248.
6. Strawa, A. W., and Cantwell, B. J., "Visualization of the Structure of a Pulsed Methane-Air Diffusion Flame," *Physics of Fluids* **28** (1985) 2317-2320.
7. Lewis, G. S., Cantwell, B. J., Vandsburger, U., and Bowman, C. T., "An Investigation of the Structure of a Laminar Non-Premixed Flame in an Unsteady Vortical Flow," *Twenty-Second Symposium (International) on Combustion*, The Combustion Institute, Pittsburgh (1988) pp. 515-521
8. Santoro, R. J., Semerjian, H. G., and Dobbins, R. A., "Soot Particle Measurements in Diffusion Flames," *Combustion and Flame* **51** (1983) 203-218.
9. Smyth, K. C., Harrington, J. E., Johnsson, E. L., and Pitts, W. M., "Greatly Enhanced Soot Scattering in Flickering CH_4 / Air Diffusion Flames," *Combustion and Flame* **95** (1993) 229-239.
10. Shaddix, C. R., Harrington, J. E., and Smyth, K. C., "Quantitative Measurements of Enhanced Soot Production in a Flickering Methane / Air Diffusion Flame," *Combustion and Flame* **99** (1994) 723-732.
11. Everest, D. A., Shaddix, C. R., and Smyth, K. C., "Quantitative Two-Photon Laser-Induced Fluorescence Imaging of CO in Flickering CH_4/Air Diffusion Flames," *Twenty-Sixth Symposium (International) on Combustion*, The Combustion Institute, Pittsburgh (1996) pp. 1161-1169.
12. Smyth, K. C., Shaddix, C. R., and Everest, D. A., "Aspects of Soot Dynamics as Revealed by Measurements of Broadband Fluorescence and Flame Luminosity in Flickering Diffusion Flames," *Combustion and Flame* **111** (1997) 185-207.
13. Shaddix, C. R., and Smyth, K. C., "Laser-Induced Incandescence Measurements of Soot Production in Steady and Flickering Methane, Propane, and Ethylene Diffusion Flames," *Combustion and Flame* **107** (1996) 418-452.
14. Pitts, W. M., "Thin-Filament Pyrometry in Flickering Laminar Diffusion Flames," *Twenty-Sixth Symposium (International) on Combustion*, The Combustion Institute, Pittsburgh (1996) pp. 1171-1179.
15. Pitts, W. M., Smyth, K. C., and Everest, D. A., "Effects of Finite Time Response and Soot Deposition on This Filament Pyrometry Measurements in Time-Varying Diffusion Flames," *Twenty-Seventh Symposium (International) on Combustion*, The Combustion Institute, Pittsburgh (1998) pp. 563-569.
16. Skaggs, R. R., and Miller, J. H., "Tunable Diode Laser Absorption Measurements of Carbon Monoxide and Temperature in a Time-Varying, Methane/Air, Non-Premixed Flame," Twenty-Sixth

Symposium (International) on Combustion, The Combustion Institute, Pittsburgh (1996) pp. 1181-1188.
17. Zhang, J., and Megaridis, C. M., "Soot Microstructure in Steady and Flickering Laminar Methane/Air Diffusion Flames," *Combustion and Flame* **112** (1998) 473-484.
18. Smyth, K. C., "Diffusion Flame Measurements of Species Concentrations, Soot Concentrations, Temperature, and Velocity," http://www.bfrl.nist.gov/865/flamedata/.
19. Kaplan, C. R., Shaddix, C. R., and Smyth, K. C., "Computations of Enhanced Soot Production in Time-Varying CH_4/Air Diffusion Flames," *Combustion and Flame* **106** (1996) 392-405.
20. Madsen, A. H., and McCluskey, D. R., "On the Accuracy and Reliability of PIV Measurements," *Seventh International Symposium on the Application of Laser Techniques to Fluid Mechanics*, July 11-14, 1994, Lisbon, Portugal.
21. Private communication with Dr. Kermit C. Smyth, December, 2000.